Bioorganic & Medicinal Chemistry 22 (2014) 6885–6892

Contents lists available at ScienceDirect

Bioorganic & Medicinal Chemistry

journal homepage: www.elsevier.com/locate/bmc

Design of a hydrogen peroxide-activatable agent that specifically targets cancer cells

Anish K. Vadukoot [a], Safnas F. AbdulSalam [a], Mark Wunderlich [b], Eboni D. Pullen [a], Julio Landero-Figueroa [a], James C. Mulloy [b], Eddie J. Merino [a,*]

[a] Department of Chemistry, University of Cincinnati, Cincinnati, OH 45221-0172, United States
[b] Division of Experimental Hematology and Cancer Biology, Cincinnati Children's Hospital Medical Center, Cincinnati, OH, United States

ARTICLE INFO

Article history:
Received 25 August 2014
Revised 10 October 2014
Accepted 19 October 2014
Available online 30 October 2014

Keywords:
Reactive oxygen species
Conjugate addition
Acute myeloid leukemia
Oxidative stress
Anti-cancer agent

ABSTRACT

Some cancers, like acute myeloid leukemia (AML), use reactive oxygen species to endogenously activate cell proliferation and angiogenic signaling cascades. Thus many cancers display increases in reactive oxygen like hydrogen peroxide concentrations. To translate this finding into a therapeutic strategy we designed new hydrogen peroxide-activated agents with two key molecular pharmacophores. The first pharmacophore is a peroxide-acceptor and the second is a pendant amine. The acceptor is an *N*-(2,5-dihydroxyphenyl)acetamide susceptible to hydrogen peroxide oxidation. We hypothesized that selectivity between AML and normal cells could be achieved by tuning the pendant amine. Synthesis and testing of fourteen compounds that differed at the pendent amine led to the identification of an agent (**14**) with 2 μM activity against AML cancer cells and an eleven fold-lower activity in healthy CD34+ blood stem cells. Interestingly, analysis shows that upon oxidation the pendant amine cyclizes, ejecting water, with the acceptor to give a bicyclic compound capable of reacting with nucleophiles. Preliminary mechanistic investigations show that AML cells made from addition of two oncogenes (NrasG12D and MLL-AF9) increase the ROS-status, is initially an anti-oxidant as hydrogen peroxide is consumed to activate the pro-drug, and cells respond by upregulating electrophilic defense as visualized by Western blotting of KEAP1. Thus, using this chemical approach we have obtained a simple, potent, and selective ROS-activated anti-AML agent.

1. Introduction

Cytotoxic molecules hold a privileged position as anti-cancer agents. These agents include compounds that damage DNA to modify cellular genetic information and natural products that induce cytotoxicity in cancer cells.[1,2] Several natural products are reactive with cellular biomolecules at very low concentrations and selectively affect cancer cells without harming normal cells.[3] Two recently identified reactive natural products, parthenolide[4,5] (PTL) and piperlongmine[6,7] (PLG), extend life in mouse models of aggressive cancers. Both these natural products modify protein targets through a conjugate addition reaction as part of their mechanism of action. It is thought that these natural products react with proteins involved in anti-oxidant synthesis and thereby selectively eliminate cells with high concentrations of reactive oxygen species (ROS).[4–7] For this project these two natural products are a benchmark from which to compare new designs.

We hypothesized that simple anti-cancer agents that simply act through a conjugate addition would be more difficult to design due to in vivo metabolism and off-target effects thus we focused on a pro-drug strategy.[8–10] Certain cancer cells, for example acute myeloid leukemia (AML) cells, have elevated levels of ROS.[11,12] At the biochemical level, ROS molecules catalyze formation of disulfide bonds or sulfinic acids to alter proteins and subsequent activity responsible for growth and angiogenesis.[13–17] For example, tumor cells from approximately 60% of patients with AML show elevated ROS; in some cases, a 100-fold elevation is observed.[18] This increased ROS is ripe for exploitation via a pro-drug strategy (Fig. 1).[19–21] In this manuscript we have designed novel pro-drugs that are unreactive until oxidized by hydrogen peroxide. Once oxidized, the molecules, like the two natural products, are capable of a conjugate addition reaction.[9,19]

We altered the design of our previous superoxide-sensitive agents such that they would react via conjugate addition upon hydrogen peroxide oxidation. A recent manuscript shows that induction of novel adducts changes anti-cancer activity and targets cancers.[22] The previous agents we designed possess

* Corresponding author.

http://dx.doi.org/10.1016/j.bmc.2014.10.029
0968-0896/

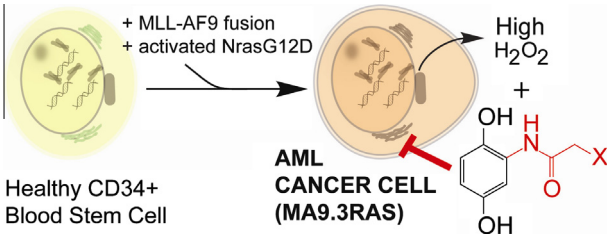

Figure 1. Design of hydrogen peroxide-activatable anti-cancer agents based on conjugate addition. AML is thought to be addicted to elevated levels of ROS, thus we have designed new agents that are activated by hydrogen peroxide. In this manuscript, blood stem cells from healthy donors are transformed into faithful models of AML by addition of two genes: an MLL-AF9 fusion and active NrasG12D. To implement the design of hydrogen peroxide-activatable agents a linker (red) on an oxidation-prone hydroquinone was installed to enforce conjugate addition after hydrogen peroxide oxidation. "X" represents α-substituent of the acetamide.

mid-nanomolar activity against some tumor cells and up to 10-fold selectivity for AML cells.[8,9] Upon oxidation, the compound reacts by 1,2-addition with an amine identified as essential. We envisioned a hydrogen peroxide-activatable agent that reacts via conjugate addition could be designed by migrating this amine and its tether ortho to the hydroxyl group of the hydroquinone (Fig. 1 red structure). This would cause the electrophilic center generated upon hydrogen peroxide activation to be C5. This change thereby facilitates hydrogen peroxide-activated conjugate addition since it utilizes quinone chemistry. In order to facilitate synthesis and identify an agent with low micromolar activity we chose an amide linker. As you will see this design led to a lead compound with a surprising mechanism of activation but still is a hydrogen peroxide-activatable agent that reacts via formation of a conjugate addition product.

As a starting point for our analysis, we synthesized compounds **1**–**14** (Table 1). Compound **14** has an IC_{50} value of 2 μM against AML cancer cells. Upon hydrogen-peroxide induced oxidation, **14** formed a bicyclic ring that equilibrated between an electrophilic oxidized and a reduced relatively stable state. Hydrogen peroxide activated the compound by more than 150-fold. Incubation with *N*-acetylcysteine leads to formation of a conjugate addition product. Cellular testing showed that our AML model system possesses more ROS than normal blood stem cells from healthy donors and the addition of **14** consumes ROS as part of its mechanism since it is essentially an anti-oxidant. Importantly, **14** is 11-fold selective and activates AML cells electrophilic defense system consistent with the hypothesized mechanism of action.

Table 1
Activity of compounds against AML cell line MA9.3RAS

	Structure	IC_{50} (μM)		Structure	IC_{50} (μM)
1	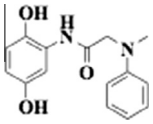	6 ± 1	**8**	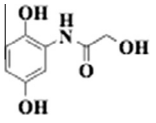	12 ± 3
2	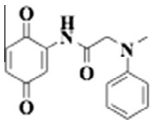	21 ± 4	**9**	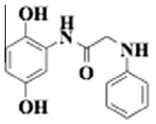	13 ± 2
3	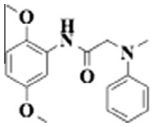	> 100	**10**	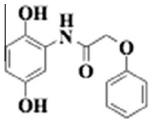	3 ± 1
4	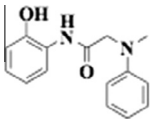	> 100	**11**	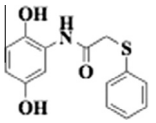	5 ± 1
5	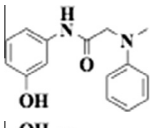	>100	**12**	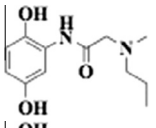	18 ± 2
6	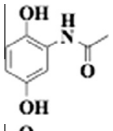	35 ± 5	**13**	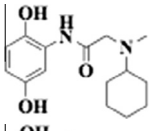	9 ± 2
7	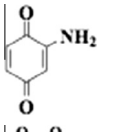	16 ± 2	**14**	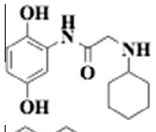	2 ± 1
PLG	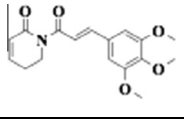	2 ± 1	**PTL**	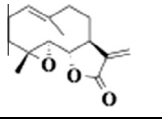	3 ± 1

2. Results

2.1. Design and reactivity of compound 1

To begin the molecular design process we synthesized compound **1** (Fig. 1). After synthesizing **1** we examined its oxidation. Two aspects of the design were of concern based on previously published studies of similar compounds. First, oxidation could form either the 1,4-quinone or an α-substituted-*N*-arylacetamide. Second, because of the many tautomers, several positions could serve as the electrophilic center. To identify the oxidation product of **1**, (diacetoxyiodo)benzene was used as a model oxidizer (Fig. 2B). The product after two-electron and concurrent two-proton oxidation was isolated and found to be **2** based on ^{1}H NMR. ^{1}H NMR showed a broad singlet at 9.75 ppm confirming the presence of amide proton and the formation of 1,4 quinone rather than α-substituted-*N*-arylacetamide. The next step in the reaction is the conjugate addition. As a test reaction the substrate *N*-acetylcysteine was incubated in dimethylsulfoxide (DMSO) along with **2** for 2 h. After isolation, NAC-2 was characterized by ^{1}H NMR (Fig. 2B). The spectrum revealed that addition occurred at C5. Singlets were observed at 7.83 ppm for H_1 and 6.85 ppm for H_2. If the addition had happened at C6, doublets due to *meta* coupling between H_3 and H_5 protons would have been present in the spectrum. Figure 2A shows the proposed reaction pathway: oxidation, conjugate addition, and regeneration of aromaticity.

To mimic cellular addition, **1** was incubated in PBS with limiting *N*-acetylcysteine and the products were analyzed by HPLC (Fig. 2C). The limiting *N*-acetylcysteine was necessary due to the formation of multiple addition products since addition of a thiol to the aromatic ring makes further oxidation and addition easier. Compound **1** was converted to **2** in the absence of exogenous oxidant at a rate of 0.011 ± 0.002 min^{-1} (Fig. 2D, grey line), which leads to approximately 50% conversion in one hour. Please note that background oxidation is dependent on molecular oxygen as reactions under argon show no oxidation (Supporting information, Fig. 5). We then assessed the ROS-induced activation of **1**. In the presence of 10 mM H_2O_2, a ten-fold excess, the rate of conversion was enhanced by more than 60-fold to 0.6 ± 0.1 min^{-1}. Once **2** was formed *N*-acetylcysteine was added and **NAC-2** was rapidly produced (Fig. 2C, black line) as confirmed by FTMS (Fig. 2E). Thus, **1** is activated by ROS, supporting our hypothesis that this agent will react with biomolecules in cells under higher oxidative stress.

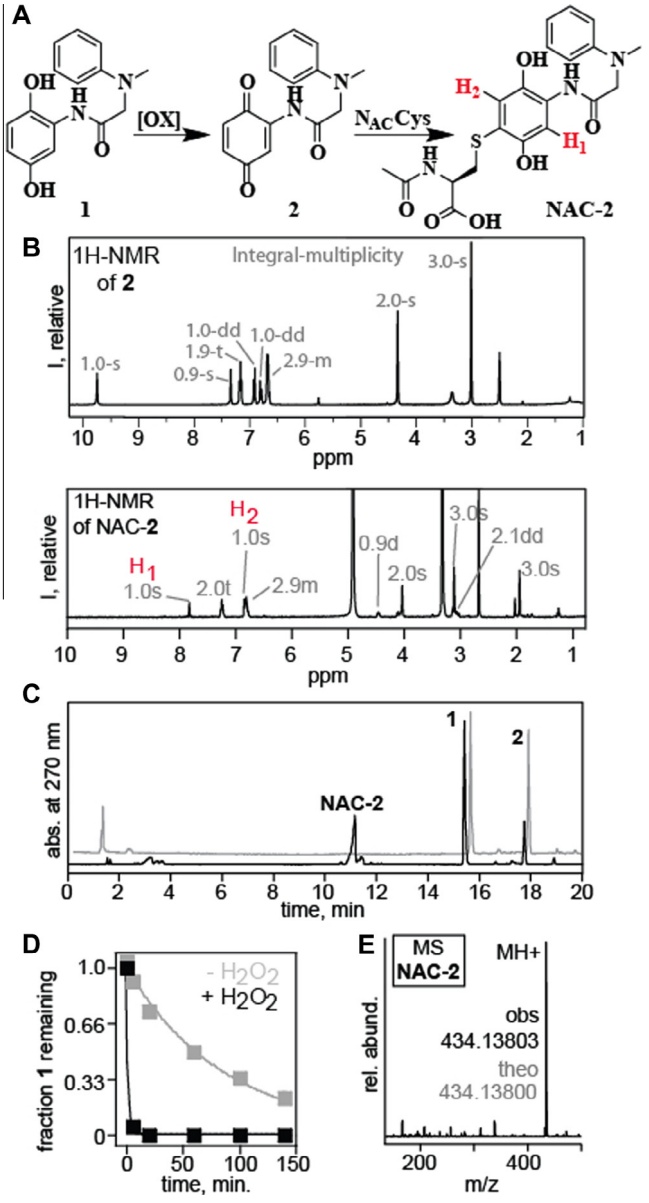

Figure 2. Reactivity of **1**. (A) The proposed reaction pathway. Oxidation of **1** leads to a quinone. In the presence of a nucleophile, like *N*-acetylcysteine, a conjugate addition reaction followed by an elimination results in the aromatic **NAC-2** species. (B) ^{1}H NMR of **2** (upper) and **NAC-2** (lower). The two red proton shifts do not show multiplicity indicating that *N*-acetylcysteine has added to C5. (C) HPLC analysis of reaction products in the absence of **NAC** (grey) and upon addition of **NAC** (black). The peak at 11.2 mins was identified as the **NAC-2** adduct. (D) Hydrogen peroxide increases the rate of conversion of **1** into **2** to 0.6 min^{-1}, an enhancement of at least 60-fold. (E) FTMS of **NAC-2**.

2.2. Structure–activity relationship

We then began to probe structural components within **1** and optimize its potency. The goal was to obtain activity that matched the two natural products, PTL and PLG that show efficacy in tumor xenografts in mice.[4,6] As a model system we evaluated cytotoxicity of synthesized agents in the MA9.3RAS AML cell line. These cells are transformed CD34+ human blood stem cells engineered to express both an MLL-AF9 fusion protein and the common oncogene NrasG12D. Culturing was accomplished as previously described.[23] The molecular signatures associated with these cells closely mimic those identified in primary AML patient samples and the MLL-fusion is associated with poor survival.[24] Cytotoxicity studies were performed in triplicates using an MTT cell proliferation assay. All MTT assays were repeated twice.

We evaluated the ROS-activated portion of the molecule as shown in Table 1. Compound **1** had an IC_{50} value (i.e., concentration at which only 50% of the AML cells survive) of 6 ± 1 μM. Oxidation within cells was necessary for activity since the IC_{50} of **2** was 21 ± 4 μM. In support of the requirement for cellular oxidation, compound **3**, which is not readily oxidized into the corresponding quinone due to the presence of methoxy groups had an IC_{50} greater than 100 μM. Compounds **4** and **5**, each lacking a single phenol at positions 2 and 5, respectively, also had IC_{50} values greater than 100 μM, showing the importance of both hydroxyl groups. Replacement of a hydroxyl group with hydrogen makes oxidization much less favorable. Analysis of these compounds indicated that oxidation was a prerequisite for high activity. Thus, these data support that to obtain a cytotoxic compound a key requirement is the ability of the compound to be oxidized.

Molecular requirements of 'X' functionality (α-substituent of the acetamide, Fig. 1) were next assessed in compounds **6**–**14** (Table 1). In compound **6**, the *N*-methylaniline of **1** was replaced with hydrogen; this substitution reduced the IC_{50} by approximately 6 fold to 35 ± 5 μM. The amine-substituted **7** had an IC_{50} of 16 ± 2 μM, whereas replacement of the *N*-methylaniline with a hydroxyl group (compound **8**) resulted in an IC_{50} of 12 ± 3 μM. We then synthesized a derivative lacking the methyl on the aniline, **9**. Compared to compound **1**, **9** also had a moderate reduction in activity (IC_{50} of 13 ± 2 μM). Two isosteres, **10** and **11**, containing a phenol and thiophenol, respectively had greater activity than **9** with IC_{50} values of 3 ± 1 μM and 5 ± 1 μM. We then replaced the distal aromatic ring with alkyl groups. In **12**, substitution with an *N*-methylpropylamine reduced activity to 18 ± 2 μM. Compound **13**, an *N*-methylcyclohexylamine derivative, showed a slight reduction in potency to 9 ± 2 μM compared to **1**, but its activity is improved over **12**. The most active compound was **14**, in which the aromatic ring was replaced with a cyclohexane. Compound **14** had an IC_{50} of 2 ± 1 μM against AML cells. We chose **14** for further chemical and biochemical analysis since it met out criterion of having similar IC_{50} as the two natural products that showed efficacy.

2.3. Compound 14 displays a propensity to cyclize upon oxidation

We then examined chemical reactivity of **14**. A potential reaction scheme is shown in Figure 3A. We hypothesized that the chemistry of **14** would differ significantly from **1**. First, as a secondary aliphatic amine we envisioned a possible cyclization reaction upon oxidation. The best possibilities for cyclization via amine addition was to C1 or C3 of the phenol to generate a new six-membered ring. Additionally nucleophilic attack could occur at C2 or by a second molecule to yield a dimer. The two six membered ring possibilities are shown in Figure 3B. Thus, we probed the reaction. Representative HPLC chromatograms in the presence and absence of hydrogen peroxide are shown in Figure 3C (left hand side). Interestingly, by comparing the dark and light grey chromatograms it is observed that two products were formed (11.2 and 15.9 min elution times). These products were produced via both spontaneous and hydrogen-peroxide induced oxidation but not under an argon atmosphere (Fig. 3C right hand side). It was found that only 4 ± 3% of **14** was converted to its oxidation product in two hours under argon atmosphere. Under normal atmosphere the reaction proceeds under pseudo-zero order reaction kinetics with a $t_{1/2}$ of 155 ± 13 min (Supporting info). Importantly, addition of one molar equivalent hydrogen peroxide lead to a near instantaneous conversion to the oxidized products. Using the lower limit of $t_{1/2}$ less than 1 min leads to a large rate enhancement. Initially the two products were isolated and a high-resolution MS was obtained

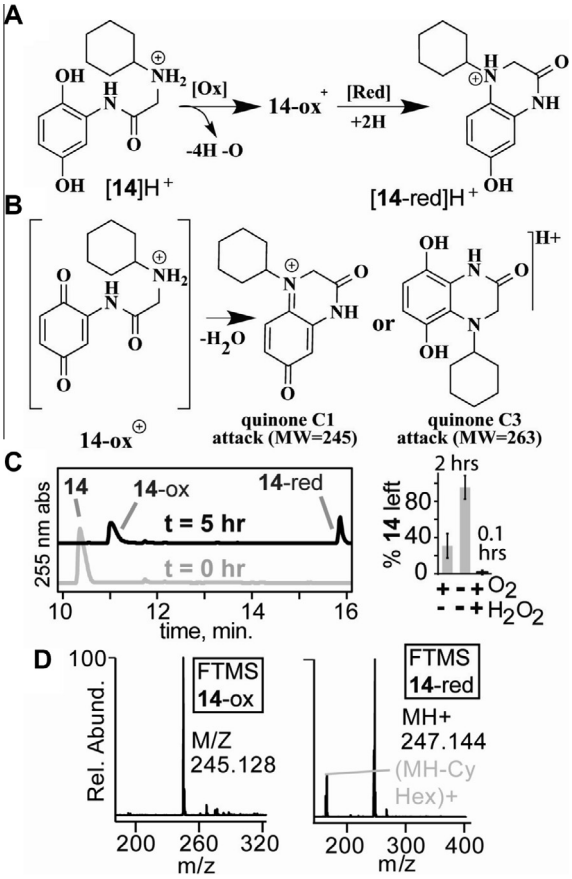

Figure 3. Oxidation of **14** leads to cyclization. (A) Proposed reaction pathway. Oxidation of **14** leads to cyclization or dimerization (not shown) to produce **14**-ox. This oxidation product can potentially reduce giving **14**-red. (B) The **14**-ox can cyclize by attack at either C1 or C3 giving products of distinct molecular weight. (C) HPLC analysis of the **14** (lower grey) and its oxidation (upper black) shows two distinct product. **14** in the absence of oxygen and peroxide is not oxidized. Two-hour exposure to the atmosphere leads to some conversion to **14**-ox while hydrogen peroxide converts all **14** in less than 0.1 h (D) Isolation and MS spectra of **14**-ox and **14**-red.

on both of them. The corresponding FTMS is shown in Figure 3D. After isolation it was found that the **14**-ox product that eluted at 11.2 min had an elemental composition of $C_{14}H_{17}N_2O_2^+$, *m*/*z* 245.148 with an error less than 100 ppb, which inferred oxidation and additionally lost H_3O^+. Please note there are several tautomers of **14**-ox possible (see Fig. 4A). Importantly, the second product (**14**-red) that eluted at 15.9 min had an elemental composition of $C_{14}H_{19}N_2O_2^+$, *m*/*z* 247.144 with an error less than 100 ppb, which was a reduction of **14**-ox.

Several critical questions remained including the tautomeric state and if thiol could add to **14**-ox. Figure 4A details six key tautomers possible from **14**-ox (numbered T1–T6). It was possible to precipitate **14**-red from aqueous solutions as neither **14**-ox nor **14**-red is stable to chromatography or heating. Thus the structure of **14**-red was identified. We then allowed **14**-red to equilibrate back to **14**-ox to identify its structure.

Important proton resonances for **14**-red are as follows. Two singlets at δ 10.24 (s, 1H) and δ 8.87 (s, 1H) correspond to the amido proton of the tether and hydroxyl group of the quinone. Aromatic protons showed up at δ 6.59 (d, J = 9.0 Hz, 1H), δ 6.35–6.30 (m, 2H). A singlet at δ 3.42 (s, 2H) ppm corresponds to protons on α-carbon next to the carbonyl group. Cyclohexylamine protons showed up at δ 3.31–3.21 (m, 1H), δ 1.77–1.59 (m, 5 H), δ 1.40–1.33(m, 4 H), δ 1.11–1.08 (m, 1H).The ^{1}H NMR is consistent with the tautomer shown in Figure 3A. Importantly, the structure

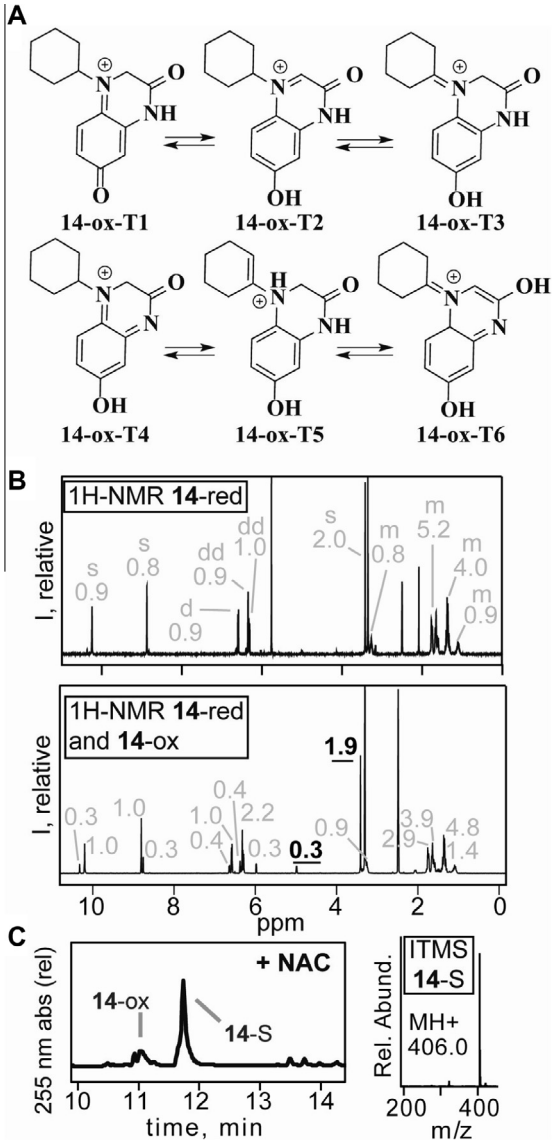

Figure 4. Oxidation of **14** leads to cyclization. (A) Proposed tautomeric structures of **14**. (B) This oxidation product can potentially reduce giving **14**-red. (Fig B first NMR) The **14**-ox can be predicted from the ^{1}H NMR of the equilibrated species (Fig. B second NMR). (C) HPLC traces of NAC- addition product with **14** and ITMS of the NAC adduct (Fig 4C left hand side).

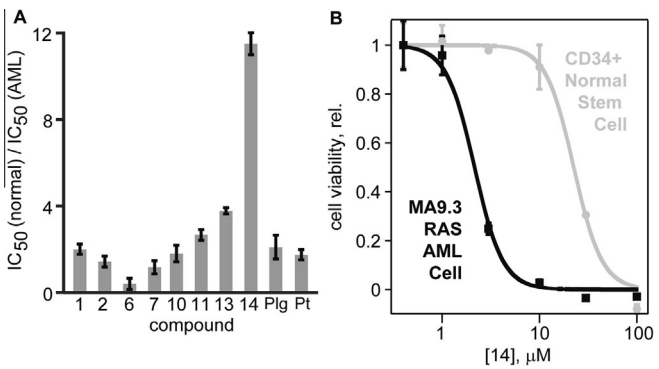

Figure 5. Compound **14** displays highly selective anti-AML activity. (A) Ratio of blood stem cell to AML activity of select synthesized agents and natural products piperlongumine (PLG) and parthenolide (PTL). (B) Viability of AML (black) and CD34+ normal blood stem cells (grey) in the presence of compound **14**.

of **14**-ox could be assigned by allowing pure **14**-red to equilibrate back into a ~25% mixture of **14**-ox. We found that it takes 1 hr for this equilibration to occur. The spectrum was normalized to the most downfield **14**-red aromatic shift at δ 6.59 ppm. By doing this it becomes apparent that there is a set of shifts corresponding to **14**-red at single proton counts and a smaller set corresponding to **14**-ox. There should be a total integration, assuming 25% **14**-ox and 75% **14**-red of 23.4 proton integration sum between the two species and we observe 23.0, well within error. The proton shifts for the **14**-ox are given as follows. Amido protons and phenolic hydroxyl are present as singlets at 10.3 and 8.48 ppm respectively with an integration of 0.3. There are three aromatic protons observed with one doublet that is shifted up-field to δ 5.58 ppm since it is adjacent to the cationic site. Since **14**-red has a total 11 protons in cyclohexyl ring, then the proton integration sum for both species should be 14.3. They are well accounted for in the spectrum. The most important and defining proton shift is the α-CH_2 group (at δ 3.39 ppm). There are supposed to be a total of 2.6 proton integration sum combined between **14**-red and **14**-ox but integrated value is 1.9 (bold and underlined in Fig. 4B, bottom NMR). This indicates that there is no α-CH_2 group present in **14**-ox. Interestingly, we observe a new shift at δ 4.98 ppm (bold and underlined in Fig. 4B, bottom NMR) similar to an allylic proton shift with an intensity of 0.3. Based on this information we can eliminate **14-ox-T3**, **14-ox-T4**, **14-ox-T5**, and **14-ox-T6** (Figure 4A) as likely structures since they lack this characteristic proton shifts. This leaves the only candidate tautomer as **14-ox-T2**. Thus, **14**-ox is likely not in a quinone state but in-fact an aromatic bicyclic ring (**14-ox-T2**). We then needed to validate that such a compound would be reactive toward nucleophile addition. As before we examined addition using *N*-acetylcysteine via HPLC (Fig. 4C). Limiting *N*-acetylcysteine was necessary due to the formation of multiple addition products as observed in HPLC and MS since the first addition leads to easier oxidation and capture of the next (thiol) nucleophile. When *N*-acetylcysteine is present a new product is observed at 12 min (**14**-S in Fig. 4C). Upon isolation and MS of **14**-S a single *m*/*z* value of 406.0 by ITMS is observed. Thus, **14** is oxidatively activated and reacts with nucleophiles.

2.4. Compound 14 has the highest selectivity among the analogs tested

The selectivity of select compounds was examined by treatment of primary CD34+ normal human blood stem cells. These are untransformed and are genetically similar to MA9.3RAS cells except they lack the MLL-AF9 oncogene and active NrasG12D oncogene. It is essential that reactive agents be selective since off-target reactivity is of great concern. In anti-cancer compounds, a selectivity factor, which in our case is the ratio between the IC_{50} of normal cells over the IC_{50} of the AML cells, of one log unit is desired. The selectivity factors for selected compounds are given in Figure 5A. Please note that MA9.3RAS and primary CD34+ normal human blood stem cells do not show different rates of cell proliferation (Supporting information, Fig. 6). Compound **1** is marginally selective with a ratio of 2.0 ± 0.2. In addition compound **2** showed similar selectivity. Active compounds, which are isosteres to **1**, **10** and **11** also had limited selectivity. Neither compound **6** nor compound **7** were selective indicating that both linker and nitrogen affect selectivity. Replacement of the aniline of **1** significantly enhanced selectivity. Conversion of the aniline to an alkyl amine led to improved selectivity. Compound **13** had a selectivity factor of 3.8 ± 1.4. Importantly, **14** was highly selective with a ratio of IC_{50} values of 11.5 ± 0.5.

We next compared **14**, the best compound, to the selectivity of two natural products that show efficacy in tumor xenografts in mice.[4,6] PLG is thought to be reactive via a conjugate addition reaction leading to a depletion of cellular antioxidant capacity. Thus, selective targeting of cancers with elevated ROS status occurs. Similarly PTL is a sesquiterpene lactone that utilizes conjugate addition. Table 1 shows that **14** has similar anti-AML activity as both these natural products. PLG has an IC_{50} of 2 ± 1 μM, while PTL has an IC_{50} of 3 ± 1 μM. Strikingly, **14** was more selective than either PLG or PTL in the MA9.3RAS AML cells as their respective selectivity were 3.7 ± 1 and 2.1 ± 0.4. When AML and control cells were treated with compound **14**, AML cells were eradicated at a concentration that did not affect viability of normal blood stem cells (Fig. 5B).

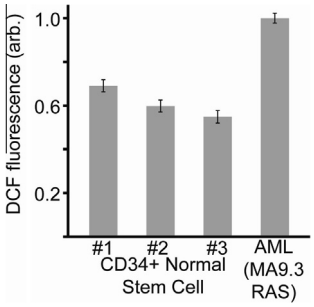

Figure 6. Compound **14** displays ROS-dependent and selective anti-AML activity. Blood stem cells from three healthy donors each show less ROS then the model AML cell line ($p < 0.01$ in all cases) as measured by a DCF fluorescence assay. (B) Addition of 20 μM **14** to AML cells leads to a time dependent loss in cellular ROS levels as measured by a DCF fluorescence assay.

2.5. Model AML cancer cells display high ROS compared to normal cells

Though it is widely accepted that bulk AML cells have elevated concentrations of reactive oxygen, we wanted to be sure that our models had higher levels of ROS than healthy cells. CD34+ blood stem cells were harvested from three donors. Cells were counted, incubated with 2,7-dihydrodichlorofluorescein (DCF) diacetate, and their respective fluorescence compared after 30 min (Fig. 6). After deacetylation DCF is oxidized by a broad spectrum of ROS species and oxidases. Thus is a marker of general ROS and oxidation within cells. The three CD34+ selected UCB cell populations each derived from different healthy donors referred as #1 through #3 (Fig. 6) had fluorescence intensity of 0.69 ± 0.03 ($p < 0.002$), 0.60 ± 0.03 ($p < 10^{-6}$), 0.54 ± 0.02 ($p < 10^{-6}$) compared to 1.00 ± 0.02 in the AML cell model.

2.6. Compound 14 reacts with cellular ROS leading to electrophilic stress

With a ROS-activatable molecule with a unique mode of reactivity, **14**, we ensured that similar events occurred within cancer cells. If **14** is ROS-activated in a cellular context it will enter a cell and react with hydrogen peroxide. Upon reaction the concentration of hydrogen peroxide will decrease. Thus examination by DCF fluorescence would show a similar effect as an anti-oxidant: lowering fluorescent signal over time (Fig. 7A). It should be noted that because **14** is highly lethal, concentrations ten-fold higher than the IC_{50} are required to lower a cell's ROS level. When **14** was added to AML cells the fluorescence intensity was set to 1.06 ± 0.13 and it smoothly increased to 4.31 ± 0.08 over time. Similar experiments lacking addition of **14** show statistically significant increases in fluorescence intensities ($p < 0.001$ for all time points while pretreated data set was not statistically significant

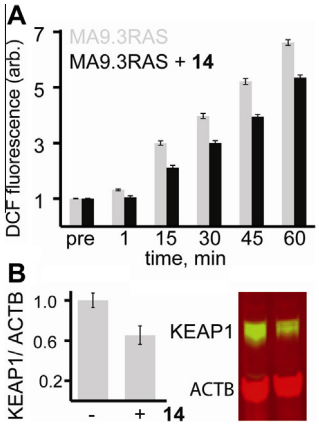

Figure 7. Compound **14** lowers ROS and leads to electrophilic stress. (A) Addition of 20 μM **14** to AML cells leads to a time dependent loss in cellular ROS levels as measured by a DCF fluorescence assay. (B) Electrophilic molecules, like **14**, are detected by a loss in concentration of the sensor protein KEAP1 ($p < 0.05$ in all cases).

from each other) with the endpoint having an intensity of 5.02 ± 0.08. Thus, **14** enters AML cells and lowers total ROS as it is activated. Finally, we wanted to assess if **14** was a reactive molecule within a cell (Fig. 7B). To accomplish this western blot against KEAP1, normalized to beta-actin was performed. KEAP1 is a signaling molecule that inhibits NRF2,[25] the transcription factor that regulates anti-oxidant concentrations in cells. Loss of KEAP1 is dependent on electrophilic and reactive stressors since it possesses several easy to modify thiols. Addition of **14** lead to a relative concentration of 0.65 ± 0.09 ($p < 0.04$) after 24 h.

3. Conclusion

In conclusion, we have synthesized a series of ROS-activatable compounds. The best compounds are cytotoxic to AML cancer cells but much less so to normal cells. The ROS-activatable portion is a simple hydroquinone. When oxidized, this module reacts with the pendant amine to form an unusual bicyclic ring. Interestingly **14** displays unique selectivity compared to its peers. We propose that this complex chemistry is integral to selectivity. Current efforts in our laboratory are focusing on optimization of this design and making this design suitable for in vivo administration via tuning of pharmacokinetic properties.

4. Material and methods for the synthesis

4.1. Synthesis

All compounds were made by divergent routes. Final compounds were prepared with more than 98% purity and characterized by ^{1}H NMR, ^{13}C NMR and HRMS. Structural characterizations for the final compounds are given below.

4.1.1. *N*-(2,5-Dihydroxyphenyl)-2-(methyl(phenyl)amino) acetamide (1)

^{1}H NMR (CD_3OD, 400 MHz) δ 7.64 (d, J = 2.91 Hz, 1H), 7.25 (dd, J = 7.12, 8.69 Hz, 2H), 6.81 (d, J = 8.30 Hz, 2H), 6.65 (d, J = 8.56, 1H), 6.41 (dd, J = 2.86, 8.61, 1H), 4.03 (s, 2H), 3.12 (s, 3H). ^{13}C NMR (CD_3OD, 400 MHz) δ 169.13 (C), 149.82 (C), 148.59 (C), 139.37 (C), 129.03 (CH), 128.98 (CH), 128.91 (CH), 125.96 (C), 119.41 (CH), 115.13 (CH), 113.83 (CH), 110.74 (CH), 107.70 (CH), 58.59 (CH_2), 39.54 (CH_3).HRMS (ESI) for $[MH]^+$ calculated: 273.12337, observed: 273.12338.

4.1.2. *N*-(3,6-Dioxocyclohexa-1,4-dienyl)-2-(methyl(phenyl)amino)acetamide (2)

^{1}H NMR (DMSO-d_6,400 MHz) δ 9.75 (s, 1H), 7.34 (d, J = 2.4 Hz, 1H), 7.17 (t, J = 8.0 Hz, 2H), 6.92 (d, J = 10.0 Hz, 1H), 6.79 (dd, J = 2.8, 10.4 Hz, 1H), 6.68–6.64 (m, 3H), 4.33 (s, 2H), 3.01 (s, 3H). ^{13}C NMR (DMSO-d_6, 400 MHz) δ 187.85 (C), 182.33 (C), 170.84 (C), 149.00 (C), 138.04 (CH), 137.79 (C), 133.25 (CH), 129.53 (CH), 119.72 (CH), 115.28 (CH), 113.90 (CH), 59.88 (CH_2), 40.41 (CH_3). HRMS (ESI) for $[MH]^+$ calculated: 271.10772, observed: 271.10771.

4.1.3. *N*-(2,5-Dimethoxyphenyl)-2-(methyl(phenyl)amino) acetamide (3)

^{1}H NMR ($CDCl_3$, 400 MHz) δ 8.96 (br s, 1H), 8.13 (dd, J = 3.2 Hz, 1H), 7.32 (d, J = 7.6 Hz, 2H), 6.89–6.84 (m, 3H), 6.76 (d, J = 9.2 Hz, 1H), 6.59 (dd, J = 3.2,8.8 Hz, 1H),4.02 (s, 2H), 3.82 (s, 3H), 3.63 (s, 3H), 3.12 (s, 3H). ^{13}C NMR ($CDCl_3$, 400 MHz) δ 169.85 (C), 153.77 (C), 149.19 (C), 143.06 (C), 128.90 (CH), 127.30 (C), 118.16 (CH), 112.93 (CH), 111.31 (CH), 108.35 (CH), 106.55 (CH), 58.20 (CH_2), 55.64 (CH_3), 54.67 (CH_3), 38.82 (CH_3). HRMS (ESI) for $[MH]^+$ calculated: 301.15467, observed: 301.15468.

4.1.4. *N*-(2-Hydroxyphenyl)-2-(methyl(phenyl)amino) acetamide (4)

^{1}H NMR ($CDCl_3$, 400 MHz) δ 9.08 (s, 1H), 8.70 (s, 1H), 7.36–7.32 (m, 2H), 7.17–7.13 (s, 1H), 7.05 (d, J = 8.4 Hz, 1H), 6.95 (t, J = 7.6 Hz, 1H), 6.87–6.81 (m, 4H), 4.04 (s, 2H), 3.12 (s, 3H).

^{13}C NMR ($CDCl_3$, 400 MHz) δ 170.65 (C), 149.15 (C), 148.82 (C), 129.62 (CH), 127.44 (CH), 124.71 (C), 122.24 (CH), 122.15 (CH), 120.39 (CH), 119.87 (CH), 113.89 (CH), 59.44 (CH_2), 40.18 (CH_3). HRMS (ESI) for $[MH]^+$ calculated: 257.12845, observed: 257.12845.

4.1.5. *N*-(3-Hydroxyphenyl)-2-(methyl(phenyl)amino) acetamide (5)

^{1}H NMR (CD_3OD, 400 MHz) δ 7.24–7.19 (m, 2H), 7.15–7.07 (m, 2H), 6.92 (d, J = 8.0 Hz, 1H), 6.78–6.71 (m, 3H), 6.54 (m, 1H), 4.05 (s, 2H), 3.08 (s, 3H). ^{13}C NMR (CD_3OD, 400 MHz) δ 170.36 (C), 157.51 (C), 149.52 (C), 138.86 (C), 129.10 (CH), 128.71 (CH), 117.37 (CH), 112.52 (CH), 111.24 (CH), 111.08 (CH), 107.30 (CH), 57.24 (CH_2), 38.85 (CH_3). HRMS (ESI) for $[MH]^+$ calculated: 257.12845, observed: 257.12845.

4.1.6. *N*-(2,5-Dihydroxyphenyl)acetamide (6)

^{1}H NMR (CD_3OD, 400 MHz) δ 7.20 (t, J = 1.6 Hz, 1H), 6.71 (dd, J = 1.6 Hz, 8.8 Hz, 1H), 6.49–6.46 (m, 1H), 2.16 (s, 3H). ^{13}C NMR (CD_3OD, 400 MHz) δ 170.70 (C), 149.86 (C), 140.85 (C), 126.21 (C), 116.36 (CH), 111.68 (CH), 109.10 (CH), 22.14 (CH_3). HRMS (ESI) for $[MH]^+$ calculated: 168.06552, observed: 168.06551.

4.1.7. 2-Aminocyclohexa-2,5-diene-1,4-dione (7)

^{1}H NMR (DMSO-d_6, 400 MHz) δ 9.22 (s, 1H), 8.96 (s, 1H), 6.67 (d, J = 8.4 Hz, 1H), 6.40 (dd, J = 2.8, 8.4 Hz, 1H), 6.33 (d, J = 2.8 Hz, 1H). ^{13}C NMR (CD_3OD, 400 MHz) δ 150.67 (C), 142.39 (C), 126.73 (C), 116.74 (CH), 112.04 (CH), 106.38 (CH). HRMS (ESI) for $[MH]^+$ calculated: 124.03930, observed: 124.03929.

4.1.8. *N*-(2,5-Dihydroxyphenyl)-2-hydroxyacetamide (8)

^{1}H NMR (CD_3OD, 400 MHz) δ 7.72 (d, J = 2.4, 1H), 6.71 (dd, J = 1.2, 8.8 Hz, 1H), 6.46–6.43 (m, 1H), 4.13 (s, 2H).^{13}C NMR (MeOD, 400 MHz) δ 171.49 (C), 149.76 (C), 139.66 (C), 125.91 (C), 115.06 (CH), 110.57 (CH), 107.37 (CH), 61.66 (CH_2). HRMS (ESI) for $[MH]^+$ calculated: 184.06043, observed: 184.06043.

4.1.9. *N*-(2,5-Dihydroxyphenyl)-2-(phenylamino)acetamide (9)

^{1}H NMR (CD_3OD, 400 MHz) δ 7.68 (s, 1H), 7.15 (t, J = 7.6 Hz, 2H), 6.73–6.60 (m, 4 H), 6.38 (d, J = 8.8 Hz, 1H), 3.85 (s, 2H). ^{13}C NMR (CD_3OD, 400 MHz) δ 170.79 (C), 149.81 (C), 147.92 (C), 139.66

(C), 128.82 (CH), 126.14 (C), 118.12 (CH), 115.09 (CH), 112.78 (CH), 110.49 (CH), 107.40 (CH), 48.86 (CH_2). HRMS (ESI) for $[MH]^+$ calculated: 259.10772, observed: 259.10773.

4.1.10. *N*-(2,5-Dihydroxyphenyl)-2-phenoxyacetamide (10)

^{1}H NMR (CD_3OD, 400 MHz) δ 7.69 (d, J = 2.98 Hz, 1H), 7.37–7.33 (m, 2H), 7.07–7.02 (m, 3H), 6.71 (d, J = 8.8 Hz, 1H), 6.44 (dd, J = 2.8, 8.4 Hz, 1H), 4.68 (s, 2H). ^{13}C NMR (CD_3OD, 400 MHz) δ 167.24 (C), 157.49 (C), 149.87 (C), 139.76 (C), 129.37 (CH), 125.76 (C), 121.77 (CH), 115.06 (CH), 114.59 (CH), 110.79 (CH), 107.68 (CH), 67.24 (CH_2). HRMS (ESI) for $[MH]^+$ calculated: 260.09173, observed: 260.09175.

4.1.11. *N*-(2,5-Dihydroxyphenyl)-2-(phenylthio)acetamide (11)

^{1}H NMR (CD_3OD, 400 MHz) δ 7.49–7.46 (m, 3H), 7.33 (t, J = 7.12 Hz, 2H), 7.27–7.23 (m, 1H), 6.67 (d, J = 8.8 Hz, 1H), 6.42 (dd, J = 3.2, 8.2 Hz, 1H), 3.84 (s, 2H). ^{13}C NMR (CD_3OD, 400 MHz) δ 167.84 (C), 149.78 (C), 140.12 (C), 134.62 (C), 129.66 (CH), 128.88 (CH), 126.82 (CH), 126.09 (C), 115.31 (CH), 110.96 (CH), 107.84 (CH), 38.52 (CH_2). HRMS (ESI) for $[MH]^+$ calculated: 276.06889, observed: 276.06892.

4.1.12. *N*-(2,5-Dihydroxyphenyl)-2-(methyl(propyl)amino) acetamide (12)

^{1}H NMR (CD_3OD, 400 MHz) δ 7.72 (dd, J = 1.2, 2.4 Hz, 1H), 6.68 (dd, J = 1.6, 8.8 Hz, 1H), 6.42–6.39 (m, 1H), 3.14 (s, 2H), 2.48 (t, J = 7.2 Hz, 2H), 2.38 (s, 3H), 1.63–1.54 (m, 2H), 0.99 (t, J = 7.2 Hz, 3H).^{13}C NMR (CD_3OD, 400 MHz) δ 170.30 (C), 149.76 (C), 139.57 (C), 126.21 (C), 114.81 (CH), 110.16 (CH), 107.13 (CH), 61.74 (CH_2), 59.71 (CH_2), 41.93 (CH_3), 20.47 (CH_2), 10.53 (CH_3).HRMS (ESI) for $[MH]^+$ calculated: 239.13902, observed: 239.13900.

4.1.13. 2-(Cyclohexyl(methyl)amino)-*N*-(2,5-dihydroxyphenyl) acetamide (13)

^{1}H NMR (CD_3OD, 400 MHz) δ 7.71 (d, J = 2.8 Hz, 1H), 6.67 (d, J = 8.4 Hz, 1H), 6.38 (dd, J = 2.8 Hz, 8.4, 1H), 3.18 (s, 2H), 2.49–2.44 (m, 1H), 2.39 (s, 3H), 1.89–1.80 (m, 4 H), 1.64 (d, J = 12.4 Hz, 1H), 1.35–1.11 (m, 5 H). ^{13}C NMR (CD_3OD, 400 MHz) δ 170.98 (C), 149.78 (C), 139.58 (C), 126.24 (C), 114.80 (CH), 110.08 (CH), 107.04 (CH), 62.96 (CH), 57.69 (CH_2), 38.02 (CH_3), 28.68 (CH_2), 25.82 (CH_2), 25.47 (CH_2). HRMS (ESI) for $[MH]^+$ calculated: 279.17032, observed: 279.17031.

4.1.14. 2-(Cyclohexylamino)-*N*-(2,5-dihydroxyphenyl) acetamide (14)

^{1}H NMR (CD_3OD, 400 MHz) δ 7.59 (s, 1H), 6.70–6.68 (m, 1H), 6.44–6.41 (m, 1H), 3.65 (s, 2H), 2.71 (t, J = 10.14 Hz, 1H), 2.03–1.99 (m, 2H), 1.83–1.80 (m, 2H), 1.68 (d, J = 12.05 Hz, 1H), 1.36–1.24 (m, 5 H). ^{13}C NMR (CD_3OD, 400 MHz) δ 163.57 (C), 149.71 (C), 140.68 (C), 125.36 (C), 115.54 (CH), 111.65 (CH), 109.16 (CH), 57.21 (CH), 45.54 (CH_2), 28.83 (CH_2), 24.61 (CH_2), 24.11 (CH_2). HRMS (ESI) for $[MH]^+$ calculated: 265.15467, observed: 265.15469.

4.2. Cellular assays

CD34+ selected Human umbilical cord blood (UCB) and MA9.3RAS AML cells were obtained from Mulloy lab at CCHMC. MA9.3RAS AML cells were cultured in IMDM 20% bovine calf serum and Human umbilical cord blood (UCB) cells were cultured in IMDM 20% bovine calf serum and supplemented with SCF, IL-3, IL-6, Flt-3L and TPO.

4.2.1. Cell cytotoxicity assay (MTT)

Cells were seeded at a density of 4×10^4 cells/well in a 96-well plate and incubated at 37 °C for overnight. Then cells were treated for 48 h with indicated concentrations of freshly dissolved compounds. The plates were centrifuged at 1500 × *g* for 5 min at 4 °C to pellet the cells and the medium containing compounds was discarded; fresh medium containing 20 μL of MTT (5 mg/mL) was added to each well and incubated for an additional 4 h. The medium was removed. After adding 200 μL of DMSO to each well, the optical densities at 575 nm were determined. Cytotoxicity data are expressed as IC_{50} values obtained from the fit to a four parameter sigmoid using the graphing software KaleidaGraph. All R^2 values were greater than 0.98 and standard errors of the three replicates were less than 20%.

4.2.2. DCF diacetate fluorescence assay

Cells in active growth phase were pelleted and dissolved in 1X HBSS to a final concentration of 4×10^5 cells/ml. 100 μl of cells were added to each well in a 96 well plate. 100 μl 1X HBSS was used as blank. DCF-DA (2′,7′-dichlorofluorescein diacetate, DCFH-DA) in 1X HBSS was added to each well to a final concentration of 10 μM and the fluorescence increase was measured (λ_{exc} = 485 nm; λ_{em} = 535 nm) with a microplate reader immediately and after 30 min incubation in 37 °C. While measuring the H_2O_2 level changes in the presence of **14**, measurements were taken after adding **14** dissolved in HBSS to a final concentration of 20 μM. Cells were incubated at 37 °C and measurements were taken in 15 min intervals for one hour. Care has been taken to control extended light exposure since DCF can undergo light induced oxidation. Data are reported as the mean ± standard deviation of six replicates. Unpaired *t*-test was performed to determine the significance. The flow rate was 1 mL/min. The injection volume for each sample was kept constant at 20 μl.

4.2.3. Western blot analysis

MA9.3RAS cells were grown to obtain a density of 1×10^6 cells/ml, splitted into two and one was treated with 0.7 μM **14** overnight. Total protein was extracted from both treated and untreated cell populations using M-PER mammalian protein extraction reagent (Thermo scientific) according to the manufacturer's protocol. The proteins were separated by 10% SDS polyacrylamide gel (precast gel purchased from Genscript) electrophoresis with a quantity of 20 μg loaded per well and transferred onto nitrocellulose membrane using Invitrogen iBlot instrument according the manufacturer's instructions. The nitrocellulose was treated according to the Western blot analysis procedure developed by LI-COR imagers. The membrane was first blocked with Odyssey blocking buffer (purchased from LI-COR) for 1 h and incubated with primary antibody mixture including rabbit anti KEAP1 mAb and mouse anti b-actin mAb for one hour followed by washing with PBS+0.1% Tween 20. The membrane was then incubated with secondary antibody mixture containing fluorescently labelled Goat anti-mouse and goat anti-rabbit antibodies and imaged by LI-COR odyssey infrared imager. Unpaired *t*-test was performed to determine the significance.

4.3. Analytical studies

4.3.1. HPLC Conditions

A Beckman Coulter's HPLC system consisting of a dual pump Model 126 with 32 Karat Software, an System Gold 168 detector and an System Gold 508 AutoSampler was used for kinetic studies. A reverse phase C-18 column (Synergi™ 4 μm Hydro-RP 80 Å, LC Column 150 × 4.6 mm, Ea) was used. The mobile phase consisted of HPLC grade Acetonitrile (Fisher Scientific) and distilled water filtered through a Millipore Milli-Q water purification system. A detection wavelength of 250 nm was used.

4.3.2. NAC-2 addition conditions

To a solution of compound **2** (0.1 g, 0.369 mmol) in dimethylsulfoxide (4.0 mL) was added *N*-acetylcysteine (0.072 g, 0.443 mmol) portion-wise. After the addition was complete the reaction was stirred at rt for 2 h. The completion of the reaction was monitored by TLC. The reaction mixture was concentrated, purified by column chromatography (10% MeOH:CH_2Cl_2) to isolate the required compound as an white solid (0.08 g, 50.0%). ^{1}H NMR (CD_3OD, 400 MHz) δ 7.83 (s, 1H), 7.26–7.23 (m, 2H), 6.85 (s, 1H), 6.83–6.78 (m, 3H), 4.49–4.44 (m, 1H), 4.04 (s, 2H), 3.14–3.01 (m, 5 H), 1.95 (s, 3H). HRMS (ESI) for $[MH]^+$ calculated: 434.13800, observed: 434.13803.

4.3.3. H_2O_2 oxidation kinetics

Compound **1** (2 mM) was freshly dissolved in 1 mL of 1XPBS. 15 μL of 10 mM H_2O_2 was added to the 1.0 mL of sample and the reaction was monitored by HPLC as per the conditions explained in 4.3.1.

4.3.4. Isolation of 14-red

10 mM concentration of compound **14** in 1XPBS was allowed to sit for 2 h, and the precipitate formed was isolated by filtration, dried under vacuum and characterized by ^{1}H NMR, ^{13}C NMR and HRMS. ^{1}H NMR (DMSO-d_6, 400 MHz) δ 10.24 (s, 1H), 8.87 (s, 1H), 6.59 (d, J = 9.0 Hz, 1H), 6.35–6.30 (m, 2H), 3.42 (s, 2H), 3.31–3.21 (m, 1H), 1.77–1.59 (m, 5H), 1.40–1.33 (m, 4H), 1.11–1.08 (m, 1H). ^{13}C NMR (DMSO-d_6, 500 MHz) δ 167.85 (C), 151.04 (C), 130.07 (C), 128.08 (C), 115.14 (CH), 109.72 (CH), 108.72 (CH), 56.90 (CH), 55.49 (CH_2), 47.35 (CH_2), 28.67 (CH_2), 26.02 (CH_2), 25.975 (CH_2). HRMS (ESI) for $[MH]^+$ calculated: 247.14410, observed: 247.14410.

Acknowledgments

This work is supported by an NIH NCI award (R21CA185370) to E.J.M. We would also like to thank the UC Technology Accelerator for funding as well as an Institutional Clinical and Translational Science Award, NIH/NCR R Grant Number 1UL1RR026314-01. This work was supported by a Translational Trials Development and Support Laboratory award (USPHS, MO1 RR 08084) and a Center of Excellence in Molecular Hematology P30 award (DK090971) to J.C.M. J.C.M. is a Leukemia and Lymphoma Society Scholar.

Supplementary data

Supplementary data associated with this article can be found, in the online version, at http://dx.doi.org/10.1016/j.bmc.2014.10.029.

References and notes

1. Delaney, J. C.; Essigmann, J. M. *Chem. Res. Toxicol.* **2008**, *21*, 232.
2. Woo, C. M.; Beizer, N. E.; Janso, J. E.; Herzon, S. B. *J. Am. Chem. Soc.* **2012**, *134*, 15285.
3. Gersch, M.; Kreuzer, J.; Sieber, S. A. *Nat. Prod. Rep.* **2012**, *29*, 659.
4. Ghantous, A.; Sinjab, A.; Herceg, Z.; Darwiche, N. Drug Discov. *Today* **2013**, *18*, 894.
5. Neelakantan, S.; Nasim, S.; Guzman, M. L.; Jordan, C. T.; Crooks, P. A. *Bioorg. Med. Chem Lett.* **2009**, *19*, 4346.
6. Raj, L.; Ide, T.; Gurkar, A. U.; Foley, M.; Schenone, M.; Li, X.; Tolliday, N. J.; Golub, T. R.; Carr, S. A.; Shamji, A. F.; Stern, A. M.; Mandinova, A.; Schreiber, S. L.; Lee, S. W. *Nature* **2011**, *475*, 231.
7. Adams, D. J.; Dai, M.; Pellegrino, G.; Wagner, B. K.; Stern, A. M.; Shamji, A. F.; Schreiber, S. L. *Proc. Natl. Acad. Sci. U.S.A.* **2012**, *109*, 15115.
8. Jones, A. R.; Bell-Horwath, T. R.; Li, G.; Rollmann, S. M.; Merino, E. J. *Chem. Res. Toxicol.* **2012**, *25*, 2542.
9. Bell-Horwath, T. R.; Vadukoot, A. K.; Thowfeik, F. S.; Li, G.; Wunderlich, M.; Mulloy, J. C.; Merino, E. J. *Bioorg. Med. Chem. Lett.* **2013**, *23*, 2951.
10. Li, G.; Bell, T.; Merino, E. J. *ChemMedChem* **2011**, *6*, 869.
11. Sallmyr, A.; Fan, J.; Datta, K.; Kim, K. T.; Grosu, D.; Shapiro, P.; Small, D.; Rassool, F. *Blood* **2008**, *111*, 3173.
12. Hu, Y.; Lu, W.; Chen, G.; Wang, P.; Chen, Z.; Zhou, Y.; Ogasawara, M.; Trachootham, D.; Feng, L.; Pelicano, H.; Chiao, P. J.; Keating, M. J.; Garcia-Manero, G.; Huang, P. *Cell Res.* **2012**, *22*, 399.
13. Abdal, D. A.; Choi, H. Y.; Kim, J. H.; Cho, S. G. *Cancers* **2010**, *2*, 859.
14. Schumacker, P. T. *Cancer Cell* **2006**, *10*, 175.
15. Reuter, S.; Gupta, S. C.; Chaturvedi, M. M.; Aggarwal, B. B. Free Radical Biol *Med.* **2010**, *49*, 1603.
16. Pereboeva, L.; Westin, E.; Patel, T.; Flaniken, I.; Lamb, L.; Klingelhutz, A.; Goldman, F. *PLoS One* **2013**, *8*.
17. Dickinson, B. C.; Chang, C. J. *Nat. Chem. Biol.* **2011**, *7*, 504.
18. Hole, P. S.; Zabkiewicz, J.; Munje, C.; Newton, Z.; Pearn, L.; White, P.; Marquez, N.; Hills, R. K.; Burnett, A. K.; Tonks, A.; Darley, R. L. *Blood* **2013**, *122*, 3322.
19. Peng, X.; Gandhi, V. *Ther Deliv.* **2012**, *3*, 823.
20. Kuang, Y.; Balakrishnan, K.; Gandhi, V.; Peng, X. *J. Am. Chem. Soc.* **2011**, *133*, 19278.
21. Major Jourden, J. L.; Cohen, S. M. *Angew. Chem., Int. Ed.* **2010**, *49*, 6795.
22. Chen, W.; Balakrishnan, K.; Kuang, Y.; Han, Y.; Fu, M.; Gandhi, V.; Peng, X. *J. Med. Chem.* **2014**, *57*, 4498.
23. Wunderlich, M.; Chou, F. S.; Link, K. A.; Mizukawa, B.; Perry, R. L.; Carroll, M.; Mulloy, J. C. *Leukemia* **2010**, *24*, 1785.
24. Wei, J.; Wunderlich, M.; Fox, C.; Alvarez, S.; Cigudosa, J. C.; Wilhelm, J. S.; Zheng, Y.; Cancelas, J. A.; Gu, Y.; Jansen, M.; Dimartino, J. F.; Mulloy, J. C. *Cancer Cell* **2008**, *13*, 483.
25. Kobayashi, A.; Kang, M. I.; Watai, Y.; Tong, K. I.; Shibata, T.; Uchida, K.; Yamamoto, M. *Mol. Cell. Biol.* **2006**, *26*, 221.